END
DATE
FILMED
8-79
DDC

② LEVEL

NAVAL POSTGRADUATE SCHOOL
Monterey, California

12 63p.

⑨ Master's

THESIS

⑥ INELASTIC ELECTRON SCATTERING FROM ^{7}Li
IN THE
VICINITY OF THE α - TRITON THRESHOLD.

Alpha

by

⑩ Robert Francis Ryan

⑪ March 1979

Thesis Advisor: Fred R. Buskirk

251450
79 07 11 052

REPORT DOCUMENTATION PAGE		READ INSTRUCTIONS BEFORE COMPLETING FORM
1. REPORT NUMBER	2. GOVT ACCESSION NO.	3. RECIPIENT'S CATALOG NUMBER
4. TITLE (and Subtitle) Inelastic Electron Scattering from ^{7}Li in the Vicinity of the α - Triton Threshold		5. TYPE OF REPORT & PERIOD COVERED Master's Thesis; March 1979
		6. PERFORMING ORG. REPORT NUMBER
7. AUTHOR(s) Robert Francis Ryan		8. CONTRACT OR GRANT NUMBER(s)
9. PERFORMING ORGANIZATION NAME AND ADDRESS Naval Postgraduate School Monterey, California 93940		10. PROGRAM ELEMENT, PROJECT, TASK AREA & WORK UNIT NUMBERS
11. CONTROLLING OFFICE NAME AND ADDRESS Naval Postgraduate School Monterey, California 93940		12. REPORT DATE March 1979
		13. NUMBER OF PAGES 62
14. MONITORING AGENCY NAME & ADDRESS(if different from Controlling Office) Naval Postgraduate School Monterey, California 93940		15. SECURITY CLASS. (of this report) Unclassified
		15a. DECLASSIFICATION/DOWNGRADING SCHEDULE

16. DISTRIBUTION STATEMENT (of this Report)

Approved for public release; distribution unlimited

17. DISTRIBUTION STATEMENT (of the abstract entered in Block 20, if different from Report)

18. SUPPLEMENTARY NOTES

19. KEY WORDS (Continue on reverse side if necessary and identify by block number)

^{7}Li; inelastic cross section; inelastic continuum; form factor

20. ABSTRACT (Continue on reverse side if necessary and identify by block number)

Inelastic electron scattering experiments were carried out on ^{7}Li within a range of momentum transfer squared of $.2 < q^2 < .65$ (F^{-2}). Inelastic cross sections and form factors were determined for the 4.55 MeV inelastic peak and the inelastic continuum caused by the disintegration of ^{7}Li into an alpha particle and a triton above the threshold of 2.45 MeV.

DD $_{1 \text{ JAN } 73}^{\text{FORM}}$ 1473   EDITION OF 1 NOV 65 IS OBSOLETE
(Page 1)   S/N 0102-014-6601 |

$.2 < sq \ q < .65 \left(\frac{1}{sqF} \right) 1$

Inelastic Electron Scattering From ^{7}Li
in the
Vicinity of the α - Triton Threshold

by

Robert Francis Ryan
Captain, United States Army
B.S., United States Military Academy, 1970

Submitted in partial fulfillment of the
requirements for the degree of

MASTER OF SCIENCE IN ENGINEERING SCIENCE

from the

NAVAL POSTGRADUATE SCHOOL
March 1979

Author _____

Approved by: _____
                                   Thesis Advisor

_____
                                   Second Reader

_____
Chairman, Department of Physics and Chemistry

_____
Dean of Science and Engineering

2

ABSTRACT

Inelastic electron scattering experiments were carried out on ^{7}Li within a range of momentum transfer squared of $.2 < q^2 < .65 (F^{-2})$. Inelastic cross sections and form factors were determined for the 4.55 MeV inelastic peak and the inelastic continuum caused by the disintegration of ^{7}Li into an alpha particle and a triton above the threshold of 2.45 MeV.

3

TABLE OF CONTENTS

LIST OF TABLES

LIST OF FIGURES

ACKNOWLEDGEMENTS

I. INTRODUCTION

Inelastic electron scattering experiments on ^{6}Li and ^{7}Li have been conducted by Bernheim and Bishop [Ref. 1, 2] in which the inelastic form factors were determined for these isotopes. These same authors [Ref. 3], as well as Hutcheon and Caplan [Ref. 4], have also investigated the inelastic form factors of the continuum at excitation energies above the α - triton threshold for ^{7}Li and above the α - deutron threshold for ^{6}Li. Bergstrom and Tomusiak [Ref. 5] of the Saskatchewan Accelerator Laboratory presented a more detailed analysis of the continuum for ^{6}Li in terms of α - deuteron disintegration.

The primary purpose of this work was to extend the detailed Saskatchewan work of Ref. 5 to the continuum of ^{7}Li. In addition, during the course of this experiment a check was made for a large inelastic peak observed but not reported by Monson [Ref. 6]. As corroborating evidence for this peak was not found, it is assumed that the scattering of electrons off the target frames which have since been modified was the cause of the apparent peak.

9

II.   THEORY

A.   ELECTRON SCATTERING

When a high energy electron is incident upon a target
material, it is scattered by the Coulomb force developed
between its negative charge and the positively charged nu-
cleus. Depending upon whether or not energy is converted
from kinetic to internal nuclear motion, the scattering
event is termed elastic or inelastic.

In elastic scattering no excitation energy is imparted
to the nucleus. The scattered electron energy is essentially
the same as the incident energy, being reduced only slightly
by the recoil of the relatively massive nucleus. If the in-
cident electron has a wavelength comparable to the size of
the nucleus (i.e. an electron with energy on the order of
100 MeV), then electron scattering experiments can be used
to study the charge distribution of the target nucleus. The
quantitative relationship is given in terms of charge form
factors discussed below.

In inelastic scattering some incident particle energy
excites the nucleus, as well as imparting recoil. The ex-
cited nucleus can assume discrete energy levels and then
decay to lower energy levels by emitting gamma rays or by
particle emission. Continuous excitation can occur when
the nucleus absorbs sufficient energy to break up into
smaller parts which can have a continuum of final state
energies.

10

B. ELASTIC SCATTERING

The differential cross section per unit solid angle for
a relativistic electron scattering elastically from a spin-
less point nucleus of charge Ze was shown by Mott [Ref. 7]
to be

$$\left(\frac{d\sigma(E_0,\theta)}{d\Omega}\right)_{Mott} \equiv \left(\frac{d\sigma(E_0,\theta)}{d\Omega}\right)_{point} = \left(\frac{Ze^2}{2E_0}\right)^2 \frac{\cos^2 \theta/2}{\sin^4 \theta/2} \cdot \frac{1}{R} \text{ , (II-1)}$$

where E_0 = incident electron energy

and $R = 1 + \frac{2 E_0}{Mc^2} \sin^2 \theta/2$ is the recoil factor for the

target nucleus of mass M   For $E_0 \ll Mc^2$, $\frac{1}{R} \approx 1$ and this term
is often omitted from the above equation. It is assumed
that the electron is extremely relativistic, that is, $E \gg mc^2$.

The Mott cross section defined above for a point nucleus
must be modified by a factor which takes into account the
finite charge distribution of the target nucleus. The square
of this charge form factor is the ratio of the observed dif-
ferential elastic cross section to the Mott cross section.

In elastic scattering the momentum transfer is $\vec{q} = \vec{p}_f - \vec{p}_0$,
where $\vec{p}_0$ and $\vec{p}_f$ are the momenta of the incident and scattered
electrons respectively. It follows that

$$\left|\vec{q}\right| = \frac{\frac{2p_0}{\hbar} \sin \theta/2}{\left[1 + \frac{2E_0}{Mc^2} \sin^2 \theta/2\right]^{\frac{1}{2}}} \approx \frac{2E_0}{\hbar c} \sin \theta/2 \text{ , (for } E_0 \ll Mc^2)$$

$$\text{(II-2)}$$

and thus q depends only upon the incident electron energy
E_0 and the scattering angle θ [Ref. 8].

For low Z elements, the plane wave Born approximations
are used in determining the cross sections for the

11

excitation of nuclear states. The plane wave Born approxima-
tion (PWBA) consists of the following three approximations:

1. First order perturbation theory is adequate to de-
scribe the interaction between the electron and the nucleus.

2. The incident and scattered electrons are treated as
plane waves.

3. Relativistic effects of the recoiling nucleus are
ignored [Ref. 9].

Considering the incident and scattered electrons as plane
waves, $\psi_o = e^{-i\vec{k}_o \cdot \vec{r}}$ and $\psi_f = e^{-i\vec{k}_f \cdot \vec{r}}$ respectively. The
differential elastic cross section is

$$
\begin{aligned}
\left(\frac{d\sigma(E_o,\theta)}{d\Omega}\right) &= \left(\frac{d\sigma(E_o,\theta)}{d\Omega}\right)_{Mott} \cdot \left| \int_{\substack{nuclear \\ volume}} \psi_f^* \, \rho(\vec{r}) \psi_o \, d^3r \right|^2 \\
&= \left(\frac{d\sigma(E_o,\theta)}{d\Omega}\right)_{Mott} \cdot \left| \int_{\substack{nuclear \\ volume}} e^{-i\vec{k}_f \cdot \vec{r}} \rho(\vec{r}) \, e^{-i\vec{k}_o \cdot \vec{r}} d^3r \right|^2 \\
&= \left(\frac{d\sigma(E_o,\theta)}{d\Omega}\right)_{Mott} \cdot \left| \frac{1}{Ze} \int_{\substack{nuclear \\ volume}} e^{-i\vec{k} \cdot \vec{r}} \rho(\vec{r}) d^3r \right|^2 .
\end{aligned}
$$

(II-3)

Since $\vec{k} = \vec{k}_f - \vec{k}_o = \frac{\vec{q}}{h}$,

$$
\left(\frac{d\sigma(E_o,\theta)}{d\Omega}\right) = \left(\frac{d\sigma(E_o,\theta)}{d\Omega}\right)_{Mott} \cdot \left|F(q)\right|^2 , \quad\quad (II-4)
$$

where $F(q) \equiv$ charge form factor. When using the PWBA for
a spin-zero nucleus, the charge form factor is thus the
Fourier transform of the nuclear charge distribution.

12

C. INELASTIC SCATTERING

The momentum transfered to the nucleus in an inelastic scattering event is a function of the incident and scattered electron energies and the scattering angle (provided that $E_O << Mc^2$), i.e.,

$$q^2 = 2 k_O^2 (1 - \cos \theta)(1 - k/k_O) + k^2$$

$$= 2\left(\frac{E_O}{\hbar c}\right)^2 (1 - \cos \theta)\left(1 - \frac{E_x}{E_O}\right) + \left(\frac{E_x}{\hbar c}\right)^2 , \qquad (II-5)$$

where $k_O = E_O/\hbar c$,

$k = E/\hbar c$,

and E_x = excitation energy.

It is possible to derive analytical expressions for the differential inelastic electron scattering cross sections using the PWBA. With these approximations the differential inelastic cross section $\left(\frac{d\sigma}{d\Omega}\right)_{PWBA}$ can be written as a sum over the cross sections for electric (e) and magnetic (m) transitions of various multipole orders:

$$\left(\frac{d\sigma}{d\Omega}\right)_{PWBA} = \sum_\lambda \left(\frac{d\sigma}{d\Omega}\right)_{e\lambda} + \sum_\lambda \left(\frac{d\sigma}{d\Omega}\right)_{m\lambda} , \qquad (II-6)$$

where

$$\left(\frac{d\sigma}{d\Omega}\right)_{e\lambda} = \alpha^2 a_\lambda q^{2\lambda} k_O^{-2} \left[\lambda(\lambda+1)^{-1} B(C\lambda, q, I_O \rightarrow I_x) V_L(\theta)\right.$$

$$\left. + B(E\lambda, q, I_O \rightarrow I_x) V_T(\theta)\right] R^{-1}$$

$$\qquad\qquad (II-7)$$

and

$$\left(\frac{d\sigma}{d\Omega}\right)_{m\lambda} = \alpha^2 a_\lambda q^{2\lambda} k_O^{-2} B(M\lambda, q, I_O \rightarrow I_x) V_T(\theta) R^{-1} . \qquad (II-8)$$

13

In these equations,

$$a_\lambda = 4\pi\lambda^{-1}(\lambda+1)\left[(2\lambda+1)!!\right]^{-2},$$

$$k_O = \frac{E_O}{\hbar c},$$

$$R = 1 + \hbar c \left(\frac{k_O}{Mc^2}\right) (1-\cos\theta),$$

λ = transition multipolarity,

α = fine structure constant,

E_O = primary electron energy,

θ = scattering angle and

M = nuclear mass.

If $E_O >> Mc^2$ for the electrons, then

$$V_L(\theta) = \tfrac{1}{2}(1+\cos\theta)/(y-\cos\theta)^2 \quad \text{and} \tag{II-9}$$

$$V_T(\theta) = \tfrac{1}{4}(2y+1-\cos\theta)/(y-\cos\theta)(1-\cos\theta) , \tag{II-10}$$

with $y = 1 + E_x^2/2E_O (E_O - E_x)$.

For $E_O >> E_x$ we have $y \rightarrow 1$ resulting in

$$V_L(\theta) = \cos^2 \theta/2 \; / \; 4\sin^4 \theta/2 \tag{II-11}$$

and
$$V_T(\theta) = 1+\sin^2 \theta/2 \; / \; 8\sin^4 \theta/2$$

$$= \cos^2 \frac{\theta}{2} (\tfrac{1}{2}+\tan^2 \frac{\theta}{2}) \; / \; 4\sin^4 \frac{\theta}{2} . \tag{II-12}$$

The R factor accounts for the effect of the recoiling
target nucleus on the final density of states. The func-
tions $V_L(\theta)$ and $V_T(\theta)$ refer to the longitudinal and trans-
verse components of the four-vector nuclear current density
resolved into components parallel and perpendicular to the
three-vector momentum transfer $\vec{q}$. The longitudinal (paral-
lel to $\vec{q}$) component represents an interaction of the elec-
tron with the nuclear charge. The transverse (perpendicular

14

to $\vec{q}$) component represents the contributions of the nuclear current and magnetization densities. $B(\lambda, q, I_o \rightarrow I_x)$ represent the reduced nuclear transition probabilities [Ref. 10].

The different angular functions $V_L(\theta)$ and $V_T(\theta)$ allow one to emphasize one type of transition over another. At backward ($\theta > 90°$) scattering angles $V_T(\theta) > V_L(\theta)$, while at forward scattering angles $V_L(\theta)$ predominates. Thus, magnetic transitions, which only involve $V_T(\theta)$ are readily identified by scattering at 180°, while electric multipole transitions dominate at forward scattering angles.

For low Z elements the PWBA given sufficiently accurate estimates of the inelastic differential cross sections. Distorted wave Born approximations (DWBA) therefore will not be discussed in this paper.

In First Born approximation, equations (II-11 and 12) reduce equations (II-7 and 8) to

$$\left(\frac{d\theta}{d\Omega}\right)_{e\lambda} = \left(\frac{d\theta}{d\Omega}\right)_{Mott} \left[F_L^2(q) + (\tfrac{1}{2} + \tan^2 \tfrac{\theta}{2}) F_T^2(q)\right] \tag{II-13}$$

and
$$\left(\frac{d\theta}{d\Omega}\right)_{m\lambda} = \left(\frac{d\theta}{d\Omega}\right)_{Mott} \left[(\tfrac{1}{2} + \tan \tfrac{\theta}{2}) F_T^2(q)\right] \tag{II-14}$$

respectively, where $F_L^2(q)$ and $F_T^2(q)$ are the inelastic form factors for the longitudinal and transverse photon absorption [Ref. 11]. By maintaining a constant q for different scattering angles by varying the incident energy, it is possible to determine $F_L^2(q)$ and $F_T^2(q)$ separately.

D. INELASTIC FORM FACTORS

In order to determine the inelastic form factors one must start by calculating the area under the elastic peak.

Two types of background must be removed from the inelastic spectrum. These include electrons which are originally scattered by the target and which subsequently scatter off the spectrometer walls and enter the detector system and the elastic peak radiation tail caused by photon emission in conjunction with nuclear scattering, plus the effects of ionization and straggling.

If one assumes that only one photon is emitted in conjunction with the nuclear scattering event and that the PWBA is applicable, the contribution to the radiation tail caused by photon emission can be reliably evaluated. The determination of the effects of stragling are less precise and one must renormalize the entire radiation tail to fit the experimental spectrum in the region of interest [Ref. 5].

After extending the shape of the elastic radiation tail into the inelastic region and subtracting it from the experimental spectrum, the inelastic spectrum remains. The differential inelastic cross section of a narrow inelastic peak can be determined by

$$\left(\frac{d\sigma(E,\theta)}{d\Omega} \right)_{in} = \frac{A_{in}}{A_{el}} \left(\frac{d\sigma(E_o,\theta)}{d\Omega} \right)$$

$$= \frac{A_{in}}{A_{el}} \left(\frac{d\sigma(E_o,\theta)}{d\Omega} \right)_{Mott} \cdot F^2(q_o) , \qquad (II-15)$$

where $\left(\dfrac{d\sigma(E_o,\theta)}{d\Omega} \right)$ = differential elastic cross section,

A_{in} = area of inelastic peak,

A_{el} = area of elastic peak,

$\left(\dfrac{d\sigma(E_o,\theta)}{d\Omega} \right)_{Mott}$ = differential elastic Mott cross section and

16

$F^2(q_o)$ = elastic form factor

The inelastic form factor $F^2(q)$ can then be determined by

$$F^2(q) = \frac{\left(\dfrac{d\sigma(E,\theta)}{d\Omega}\right)}{\left(\dfrac{d\sigma(E_o,\theta)}{d\Omega}\right)_{Mott}} \qquad (II-16)$$

Equations (II-15) and (II-16) assume a common shape between the elastic and inelastic peaks and that the radiation corrections are the same for both elastic and inelastic scattering. The inelastic cross section is expressed as an area per unit solid angle since it is determined in terms of an integral over the inelastic peak.

In determining the inelastic cross section for the excitation of a continuum of final states the cross section is expressed in terms of an area per unit final energy per unit solid angle. After determining the area (A_{in}) by integrating over the desired energy range, the continuum cross section can be determined by equation (II-15). The continuum form factor can then be determined using equation (II-16) [Ref. 3].

17

III. EXPERIMENTAL EQUIPMENT AND PROCEDURE

A. NAVAL POSTGRADUATE SCHOOL LINEAR ACCELERATOR

The NPS 120 MeV LINAC is an electron accelerator similar to the Stanford University Mark III linear accelerator described by Chodorow et al [Ref. 13]. The NPS LINAC consists of three 10 foot accelerator sections and is powered by three klystrons, each capable of 22 megawatts peak power. The machine is pulsed at a rate of 60 pulses per second with each beam pulse having approximately one microsecond duration. The maximum average beam current is approximately one microampere.

Beam deflection magnets and energy defining slits are used to select the beam energy, which can range from 30 to 105 MeV with energy resolution of 0.3%. The energy resolution attained in the experiments reported herein was 0.6%. Target thickness is the main reason for the lower resolution. For this reason, the 478 KeV inelastic peak could not be resolved; therefore, its area is added to that of the elastic peak.

The field of the beam deflection magnet could be measured by a nuclear magnetic resonance (NMR) probe, but this probe did not function during these runs. A total of four quadrupole magnets are available to focus the beam to a diameter of approximately two millimeters at the target. In recent experiments only the last two have been used,

18

because the first pair cause the beam to expand, hit the beam
pipes and cause excess background.

B.   SPECTROMETER AND COUNTING SYSTEM

The NPS LINAC has a movable, 16-inch radius, double focus-
ing magnetic spectrometer capable of measuring electrons
scattered at angles from 45 to 150 degrees in 15 degree steps.

The energy distribution of scattered electrons is measured
by varying the field of the spectrometer magnet. Ten NE102
plastic scintillation counters located in the focal plane of
the spectrometer serve as detectors for the ten counting
channels. The spread of these counters span a range $\pm$ 1.5
percent about the spectrometer energy. Each counter thus
detects an energy spread of 0.3 percent of the central spec-
trometer energy. Two large detectors, each spanning the
same field width as the ten smaller detectors, act as dual
coincidence backing counters. An electron passing through a
front detector and both backing detectors will record one
count on the Jorway Model 1836 Dual Channel Scalar. The
accelerator gun pulse and the counter gating circuit are
synchronized so that counts are recorded only during pulses.
This prevents background counts from being counted between
pulses.

The scalars are capable of recording periodic pulses up
to 150 MHZ. However, since the beam is pulsed, the count
rate was limited to 50 counts per second in the counter
registering the elastic peak and 150 counts per second in
the back counters while scanning the inelastic area of the

19

spectrum. These count rates avoided significant count rate losses. A Faraday cup is capable of calibrating the charge collected on the Secondary Emission Monitor (SEM). Past calibrations showed less than 0.1% change in the SEM calibrations.

C. TARGETS

^{7}Li targets with thicknesses of 106.0, 147.5, and 150.0 mils were used. Since lithium reacts quickly with air to form lithium nitride, target preparation had to be conducted with the lithium immersed in an oil bath. The targets were hydraulically pressed between polished stainless steel plates separated by metal spacers to approximate the desired thicknesses. This method precludes preparing targets accurately to a predetermined thickness. Several micrometer readings of the target thickness were taken over the surface of the target. Thickness readings varied by less than 0.3 percent. The targets were mounted in an aluminum ladder and the target chamber was quickly evacuated to approximately 1.5 x 10^{-5} torr to limit target contamination. Chamber vacuum had to be released when changing the scattering angle and the targets thus became exposed to air for short periods of time. The effect of this is seen in Figures IV-4, 6, 7 and 8 which show peaks on the high energy side slope of the elastic scattering peak. This was caused by the difference in recoil of the ^{7}Li nuclei and the N nuclei. Elastic peak areas were adjusted to account for this effect.

D. DATA ACCUMULATION

Beam energy and scattering angle were kept constant dur-
ing each data accumulation run. The spectrometer energy was
decreased in 50 KeV steps over the elastic peak and in
0.1 MeV steps over the inelastic region of interest. The
integration, capacitance and beam intensity were chosen to
prevent exceeding maximum count rates discussed in Section
III-B. For the 90 MeV runs the spectrometer energy was
initially set at 100 MeV and then reduced to a starting point
approximately two MeV above the elastic peak. Elastic data
was recorded in 50 KeV steps to approximately six MeV below
the elastic peak. During the inelastic runs the beam was
retuned to give maximum intensity consistent with the above
mentioned count rate restrictions and the spectrometer energy
was returned to a starting position which showed the elastic
peak maximum registering in counting channel number ten. In
order to follow the same hysteresis loop, the spectrometer
magnet energy was returned to 100 MeV and then reduced to
the starting point energy. Inelastic data was taken in 0.1
MeV steps down to a point approximately nine MeV below the
elastic peak. A similar procedure was used for the 105 MeV
runs. In this case the spectrometer energy was initially
set at 110 MeV and then reduced to a starting point approxi-
mately 2.5 MeV above the elastic peak. Elastic data was re-
corded in 50 KeV steps to approximately seven MeV below the
elastic peak. Prior to collecting the inelastic data the
spectrometer energy was returned to 110 MeV and then to the

21

inelastic starting point as per the arguments presented
above.   Inelastic data was recorded in 0.1 MeV steps down
to a point approximately ten MeV below the elastic peak.

Incident energy, integration, machine energy, capaci-
tance, elapsed time and the counts for the ten counting chan-
nels and two back counters were automatically recorded on a
digital readout.   This data was electrically transmitted to
an IMSAI 8080 micro-computer and displayed on an ancillary
cathode ray tube (CRT) where it could be verified before
being recorded on both cassette tape and magnetic seven-
track tape.   A teletype also provided a hard copy of re-
corded data.   The magnetic tape was used to provide input
to Code ASC described in Appendix A.   The hard copy was used
in editing the data after it had been transferred from the
magnetic tape to disk storage in the NPS IBM 360 computer.
The cassette tape provided a backup and could be used to
re-record a seven-track tape if necessary.

Code ASC, which uses the input from the spectrometer
energy, counting channels, integration, capacitance and
elapsed time of each run to compute a single spectrum,
automatically corrects the energy of each counter to cor-
respond to the true energy being detected.   Relative count-
er efficiencies are therefore taken into account because
each point in the final spectrum is actually the average
of points from each counter.

22

IV. DATA ANALYSIS

A. ELASTIC SPECTRUM

The spectrum generated by Code ASC was plotted and the area under the elastic peak was determined as described below. Integration of the area under the elastic peak was carried out from the upper limit of the peak to an energy two full widths at half maximum (FWHM) down from the peak energy.

The area of the elastic peak thus obtained must be corrected for virtual and real emission and absorption of radiation during scattering. Schwinger [Ref. 14] originally developed a multiplicative correction for virtual emission and absorption assuming a recoilless target nucleus. As modified by Tsai [Ref. 15] to include recoil, thus multiplicative constant is

$$K_s = e^{\delta_s} , \qquad \qquad (IV-1)$$

where $\delta_s = \frac{2\alpha}{\pi} \left\{ \left[\ln \frac{E_i}{\Delta E R^{3/2}} - \frac{13}{12} \right] \left[\ln \left(\frac{2E_i Mc^2}{(mc^2)^2} \left(1-\frac{1}{R}\right) \right) \right] + \frac{17}{36} \right\}, \quad (IV-2)$

where α = the fine structure constant,

$\quad E_i$ = the incident electron energy,

$\quad\quad E$ = elastic peak energy (E_o) - lower cutoff energy used in determining elastic peak area,

$\quad R$ = recoil factor previously defined,

$\quad M$ = rest mass of target nucleus and

$\quad m$ = electron rest mass.

23

Bethe and Ashkin [Ref. 16] developed the correction for the emission of real radiation

$$K_b = e^{\delta_b} , \qquad\qquad (IV-3)$$

where $\delta_b = \dfrac{t_o}{\ln 2} \ln \dfrac{E_i}{\Delta ER^{3/2}}$, $\qquad\qquad (IV-4)$

$\quad t_o$ = the effective target thickness in radiation lengths,

and the other parameters are as defined for equation IV-2 above. Equation IV-4 is valid only if $\qquad\qquad$.

The elastic area then becomes

$$A(E_o) = K_s K_b\, A(E_o)\, \text{observed.} \qquad\qquad (IV-5)$$

Although background radiation was subtracted, the area due to the unresolved 478 KeV excited state was not; thus the elastic area are slightly larger. The differential elastic scattering cross section was determined using equation II-4. In this equation the $F(q)$ used was as reported by Bumiller et al [Ref. 17] as

$$F(q) = d(1-cq^2)e^{-aq^2}, \qquad\qquad (IV-2)$$

where d = 1.0,

c = 0.169 and

a = 0.713.

B. CALCULATION OF THE ELASTIC PEAK RADIATION TAIL

The radiation tail is primarily the result of radiation during scattering and radiation before or after scattering in the electromagnetic field of a different nucleus. The effect of radiation during scattering can be evaluated, as shown by Barber et al [Ref. 12], using the Schiff [Ref. 18] calculation of the differential cross section,

24

$$\frac{d^2\,\sigma_a(E)}{d\Omega} = \left(\frac{d\sigma(E_O)}{d\Omega}\right)\frac{\alpha}{\pi}\left(1 + \frac{E^2}{E_O^2}\right)\left[\ln\left(\frac{2E\,\sin\theta/2}{mc^2}\right) - \frac{1}{2}\right]$$

$$\cdot\frac{1}{(E_O-E)}\left(1 + \frac{E_O^2}{E^2}\,\frac{F^2(q)}{F^2(q_O)}\right)\,, \qquad\qquad (IV-7)$$

where $\left(\dfrac{d\sigma(E_O)}{d\Omega}\right) = \left(\dfrac{d\sigma(E_O)}{d\Omega}\right)_{Mott} \cdot F^2(q_O)$,

α = fine structure constant and

m = electron mass.

The area of the elastic peak $A(E_O)$ was determined in counts - MeV units. The spectrum of the Schiff radiation tail $N_S(E)$ in counts was determined by

$$\frac{A(E_O)}{N_S(E)} = \frac{\left(\dfrac{d\sigma}{d\Omega}(E_O)\right)}{\left(\dfrac{d^2\,\sigma_a(E)}{d\Omega}\right)} \quad\text{or}$$

$$N_S(E) = \frac{A(E_O)\left(\dfrac{d^2\,\sigma_a(E)}{d\Omega}\right)}{\left(\dfrac{d\sigma}{d\Omega}(E_O)\right)} \cdot \frac{E}{E_O}\,, \qquad\qquad (IV-8)$$

where the factor $\dfrac{E}{E_O}$ corrects for counter resolution.

The effect of radiation before or after scattering due to brehmsstrahlung is

$$\frac{d^2\,\sigma_B(E)}{d\Omega\,dE} = \frac{b_1}{2}\,\frac{1}{(E_O-E)}\left[\frac{d\sigma(E_O)}{d\Omega} + \frac{d\sigma(E)}{d\Omega}\right]\,, \ (IV-9)$$

where $b_1 = \dfrac{(\text{target thickness in radiation lengths})}{\ln 2}$.

The spectrum of the bremsstrahlung radiation tail $N_b(E)$ was then computed in a manner similar to equation IV-8 above and the sum of $N_s(E)$ and $N_b(E)$ yield the spectrum of the total radiation tail.

25

The radiation tail then had to be normalized as discussed earlier to fit the area of interest on the elastic peak's lower energy slope. The tail was normalized from 1 MeV excitation energy to the α -triton threshold at $\sim$ 2.45 MeV excitation energy. The normalized radiation tails are depicted in Figures IV-1 through 8. The noramlized radiation tail was then subtracted from the raw data spectrum to obtain the inelastic continuum as shown in Figures IV-9 through 16.

C.   INELASTIC SPECTRUM

In order to separate the inelastic peak at 4.55 MeV from the continuous inelastic spectrum, a fitting routine was used to generate a line fit to the data on either side of the inelastic peak from threshold to 6 MeV excitation energy. This line fit is represented by the dashed line in Figures IV-9 through 16. The line fit was subtracted from the spectrum in order to yield the contribution of the inelastic peak. The area of the inelastic peak was then determined and compared to the corrected elastic peak area as shown in Table IV-2. Per arguments presented in Section II-D, the elastic and inelastic peaks were assumed to have the same shape and thus the inelastic cross section can be determined by equation (II-15). The results are discussed in Section V-B and shown in Table IV-2.

The inelastic continuum cross section per unit final energy was determined by integrating the fitted line shape described above from the threshold excitation energy as a

lower limit to the desired upper limit $\leq$ 6 MeV excitation
energy. The corresponding inelastic form factors for both
the continuum and the inelastic peak were determined by
dividing the computed integrated cross sectons by the Mott
cross sectons evaluated at the appropriate incident ener-
gies. Results are presented in Tables IV-3 and 4.

D. ERROR ANALYSIS

Since the experimental cross sections and form factors
were determined by the ratio of elastic and inelastic peak/
continuum areas resulting from data accumulated during a
single run, many of the systematic errors cancelled; e.g.
target thickness, solid angle, SEM efficiency and spectro-
meter efficiency.

As mentioned earlier, the spectra of certain runs showed
evidence of nitrogen contamination which added to the elas-
tic peak area. The uncertainty in adjusting the elastic
peak areas due to this effect was estimated to be less than
0.2%.

The inability to resolve the 478 KeV level in this ex-
periment means that the elastic peak areas are too large.
Using the arguments presented by Suelze et al [Ref. 19] it
is estimated that the error introduced will be approximately
two percent at most.

The statistical error computed by Code ASC and depicted
in Figures IV-1 through 8 show that these errors were in-
significant in determining the elastic to inelastic peak
area ratios. Relatively small errors would also be introduced

by the step sizes used in the experiment and the limitations which they impose on locating the elastic and inelastic peak energies. This will have a correspondingly small effect on determining the spectrum of the radiation tail of the elastic peak.

The largest error is introduced by the combined effect of normalizing the radiation tail to the areas of the elastic peak as already described in Section IV-B, and in generating a least squares fit to the inelastic continuum from threshold to 6 MeV excitation energy. The worst case would occur at the highest q value since the integrated cross section of the continuum decreases as q increases. Since the line shape spectrum of the fitted curve is subtracted from the inelastic peak, errors which tend to increase the area of the continuum have the reverse effect on the area of the inelastic peak and vice versa. It is estimated that these effects could introduce errors into the determined inelastic cross sections and form factors of as much as $\pm 5\%$.

Figure IV-1

$\left(\dfrac{\text{σ}}{\text{dΩ}} \right)_{\text{Mott}}$ = differential elastic Mott cross section and

^{7}Li 89.22 MeV 75 DEGREES

RADIATION TAIL

ENERGY (MeV)

COUNTS (/μC)
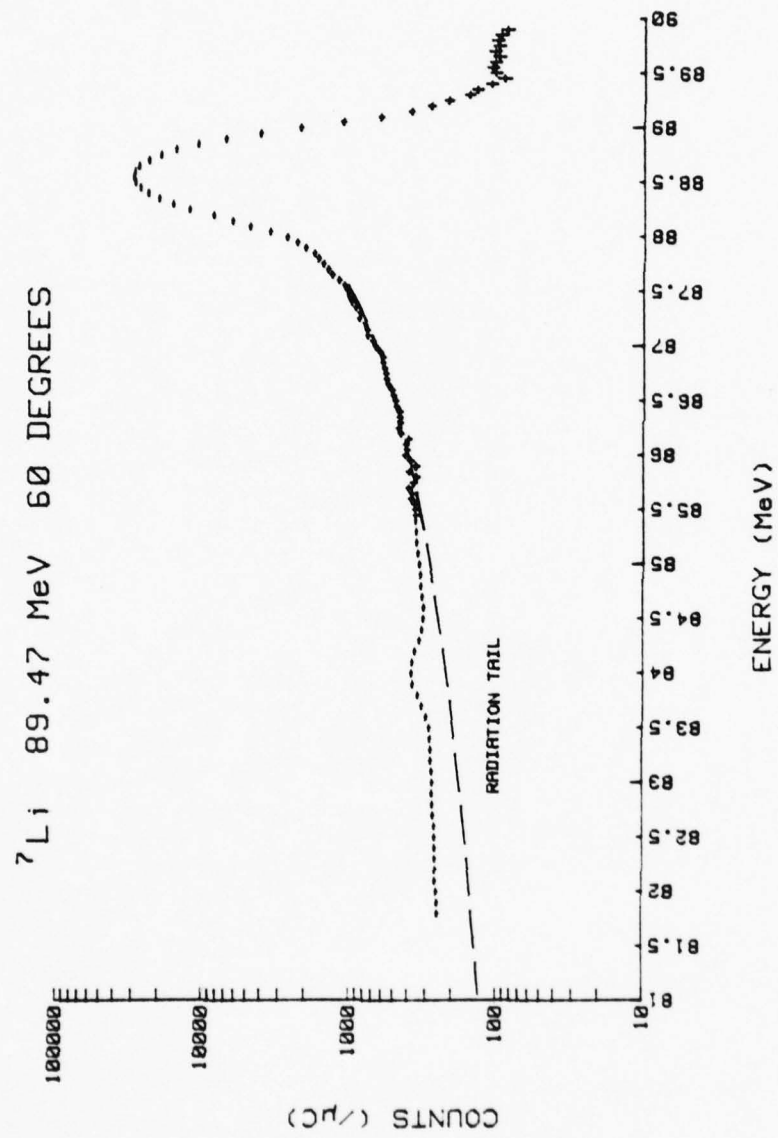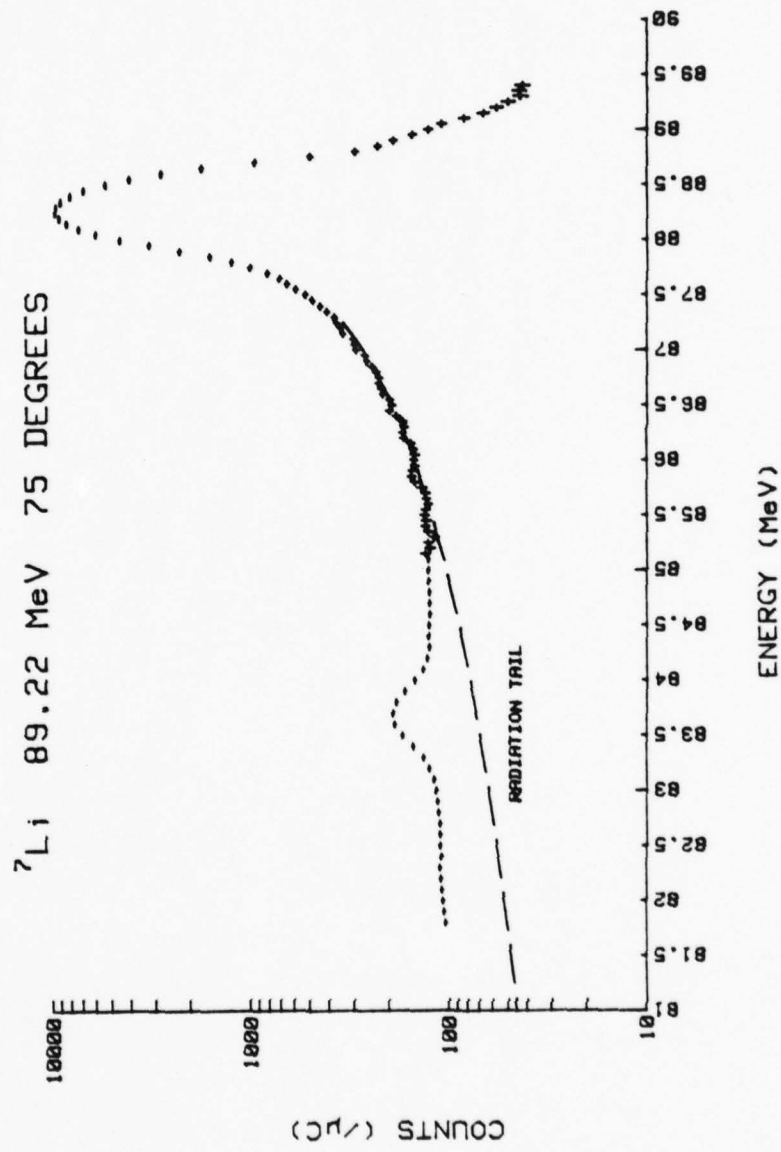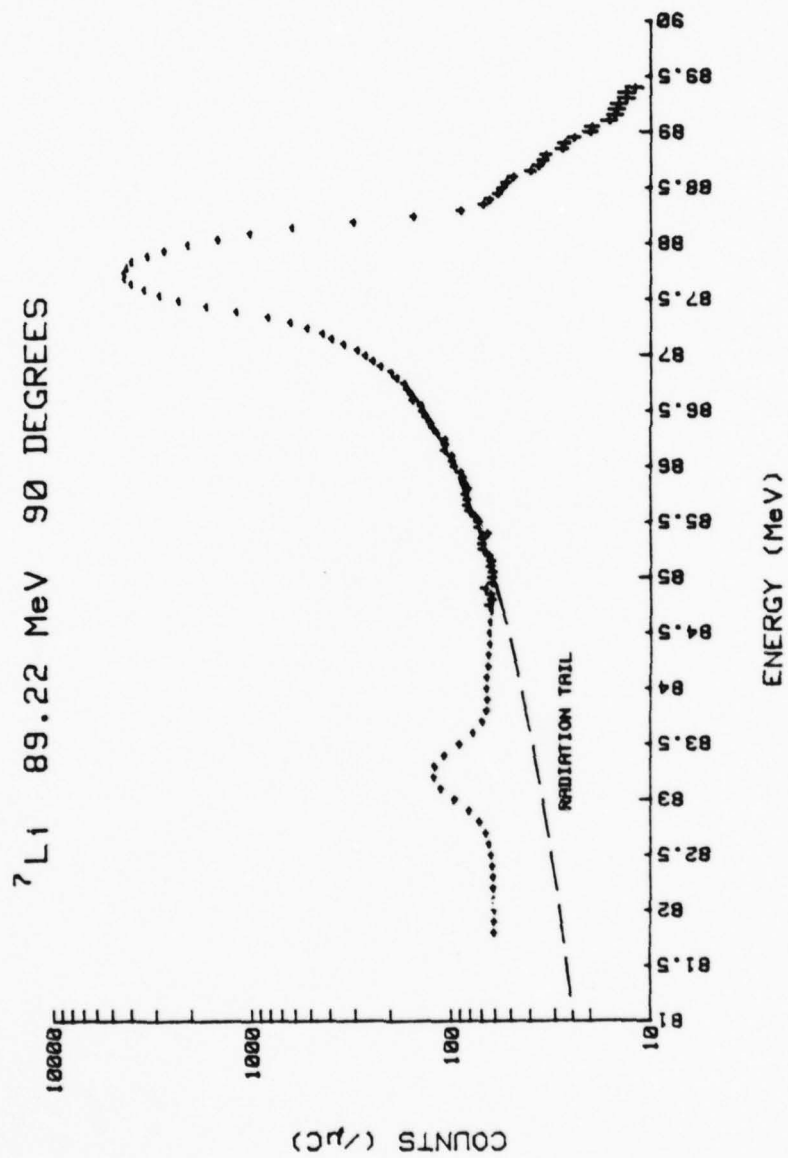
Figure IV-2
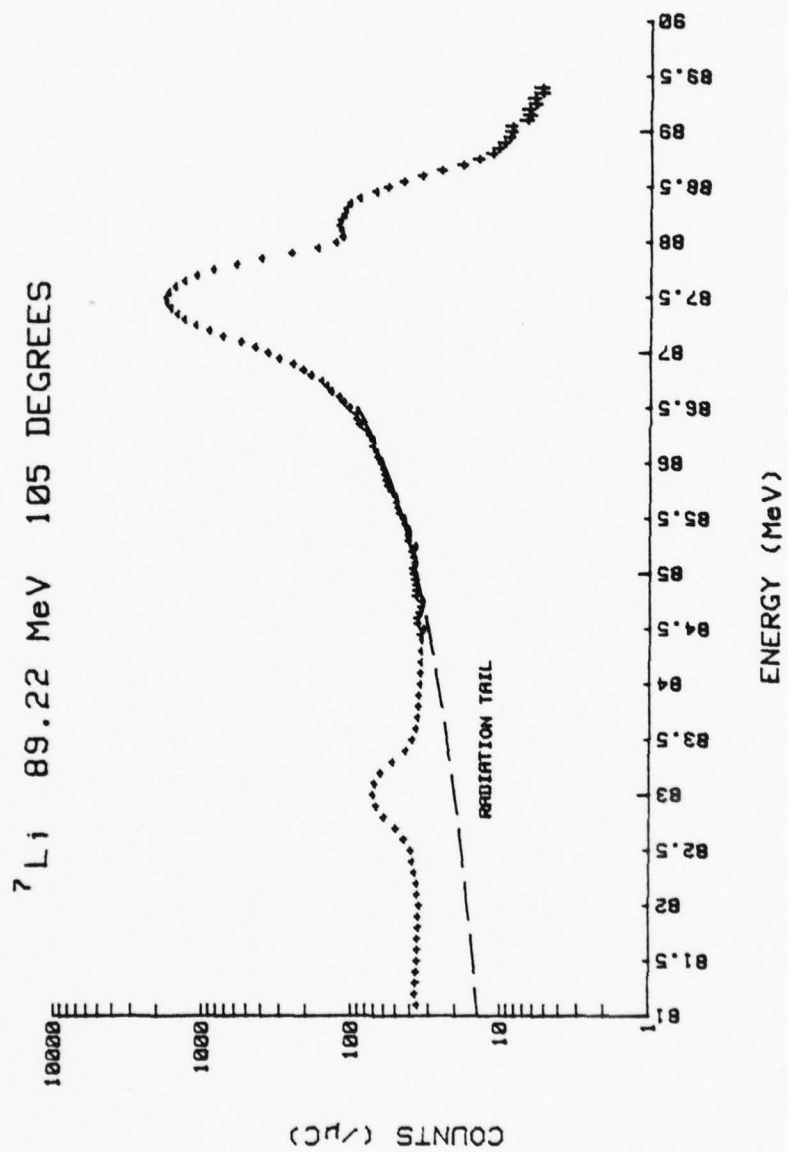
Figure IV-3

Figure IV-4
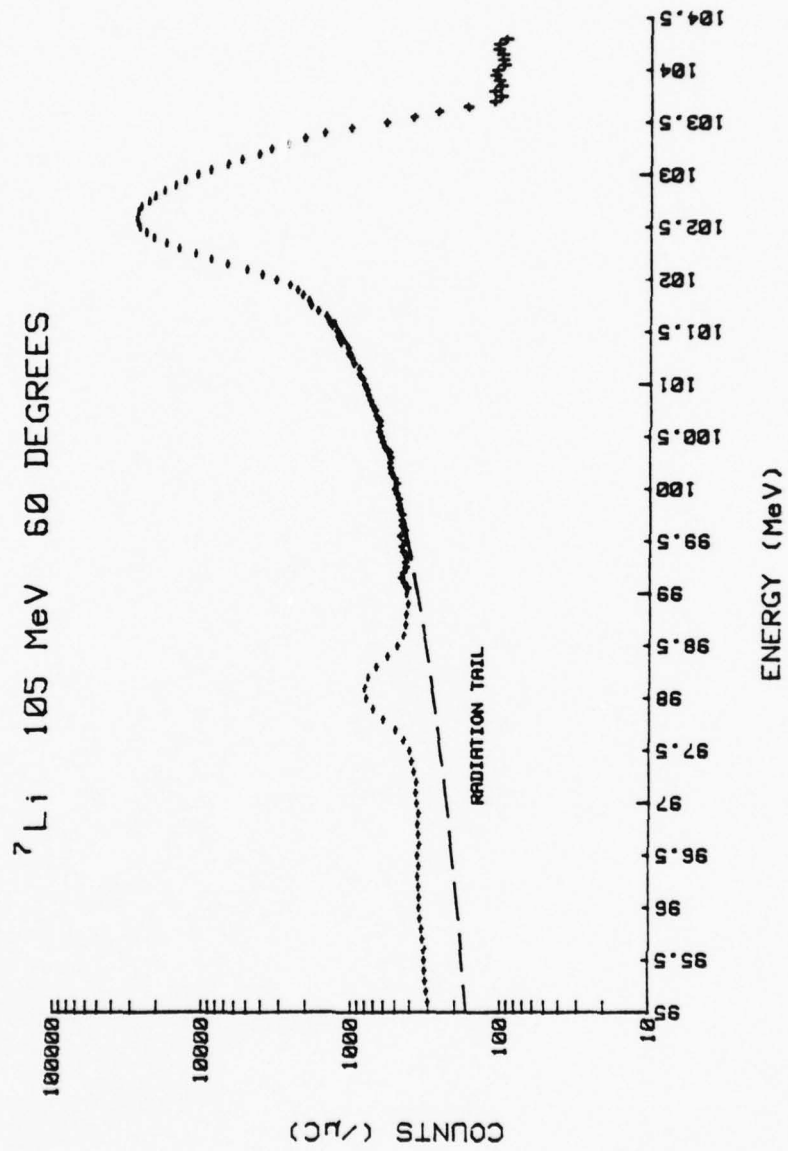
Figure IV-5
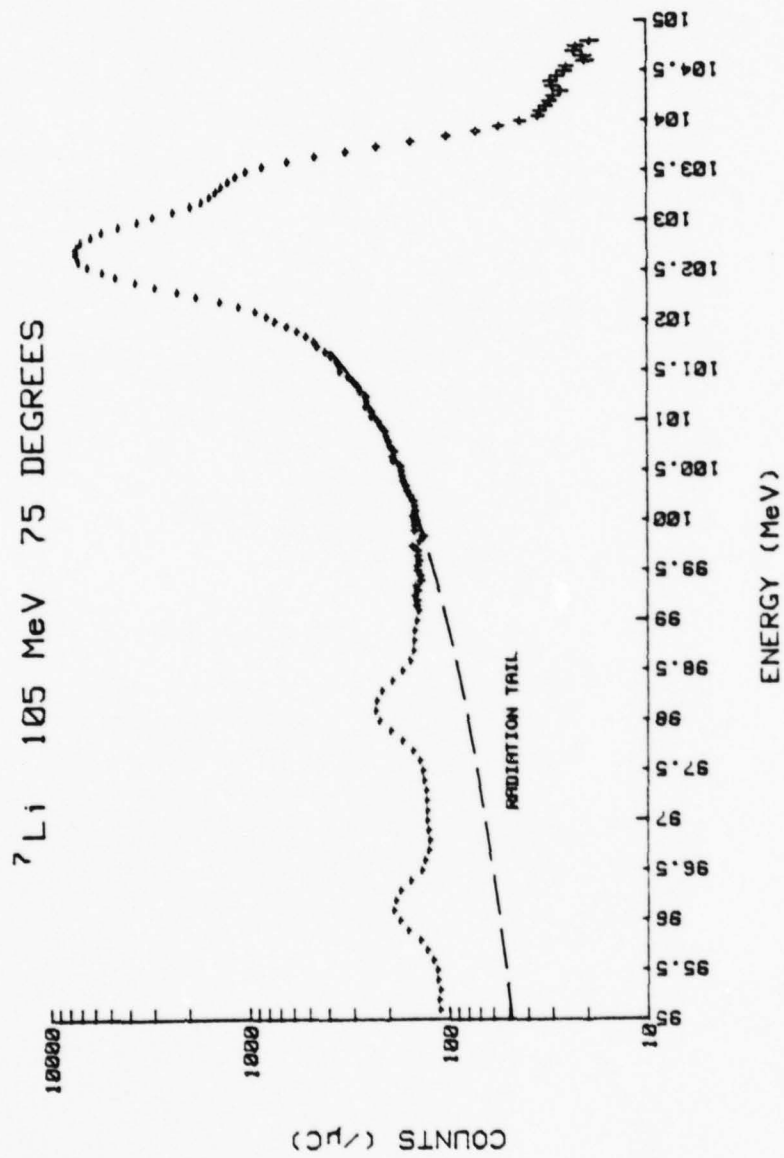
Figure IV-6
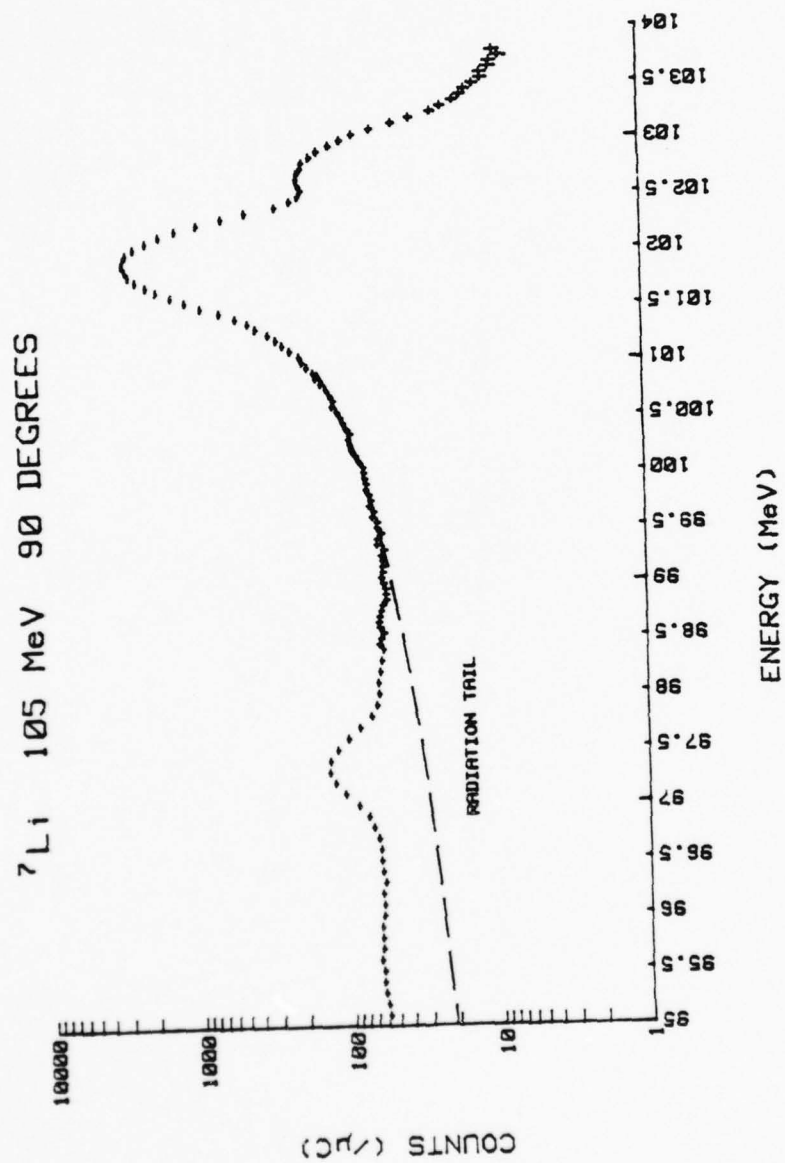
Figure IV-7
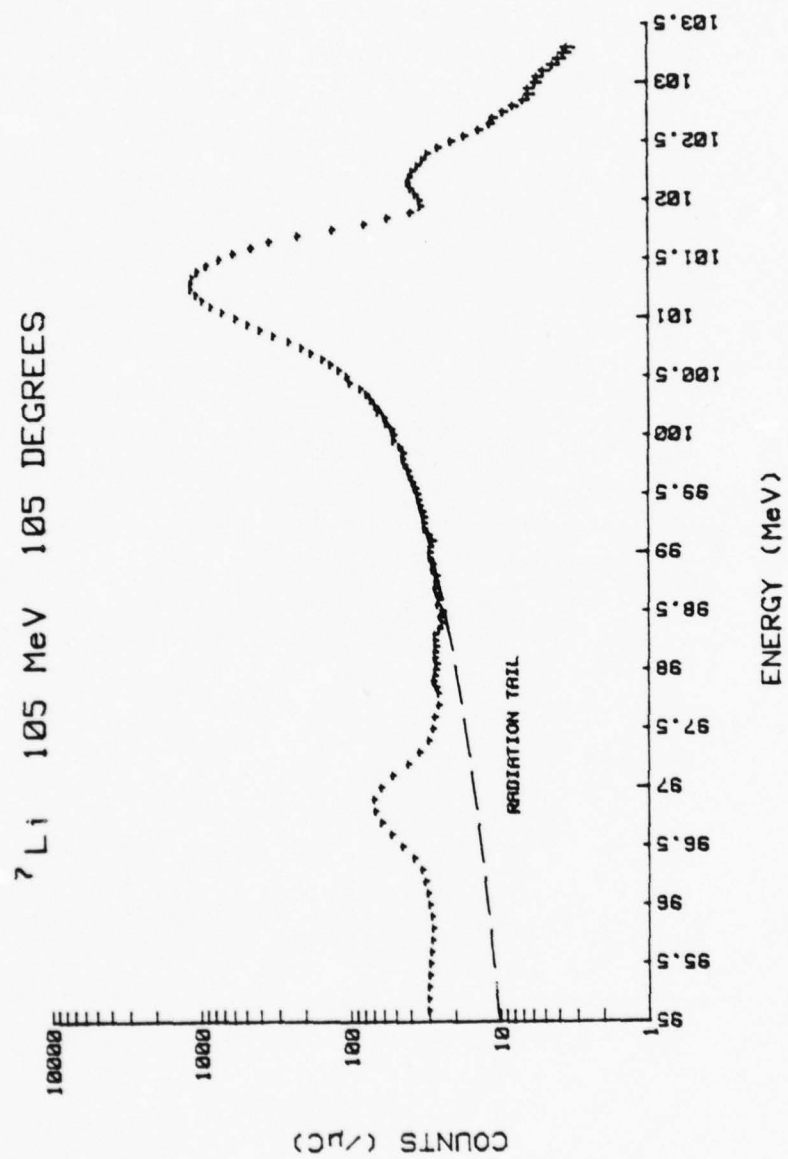
Figure IV-8
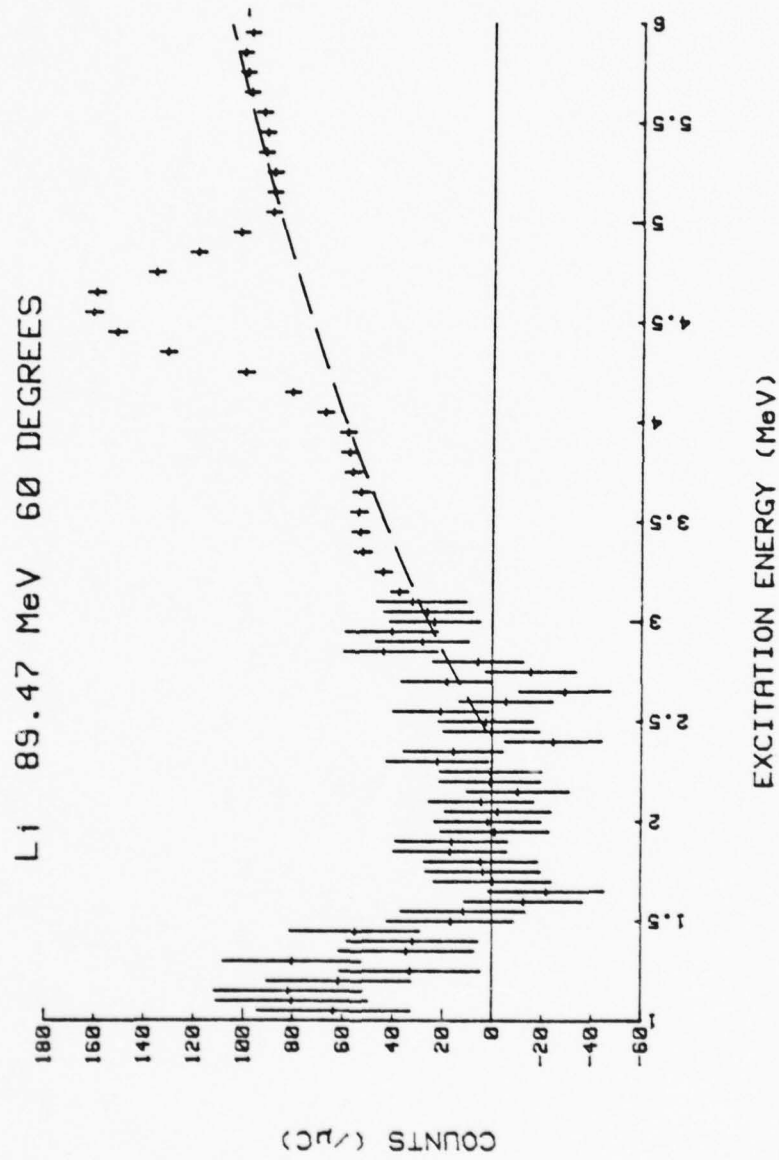
Figure IV-9
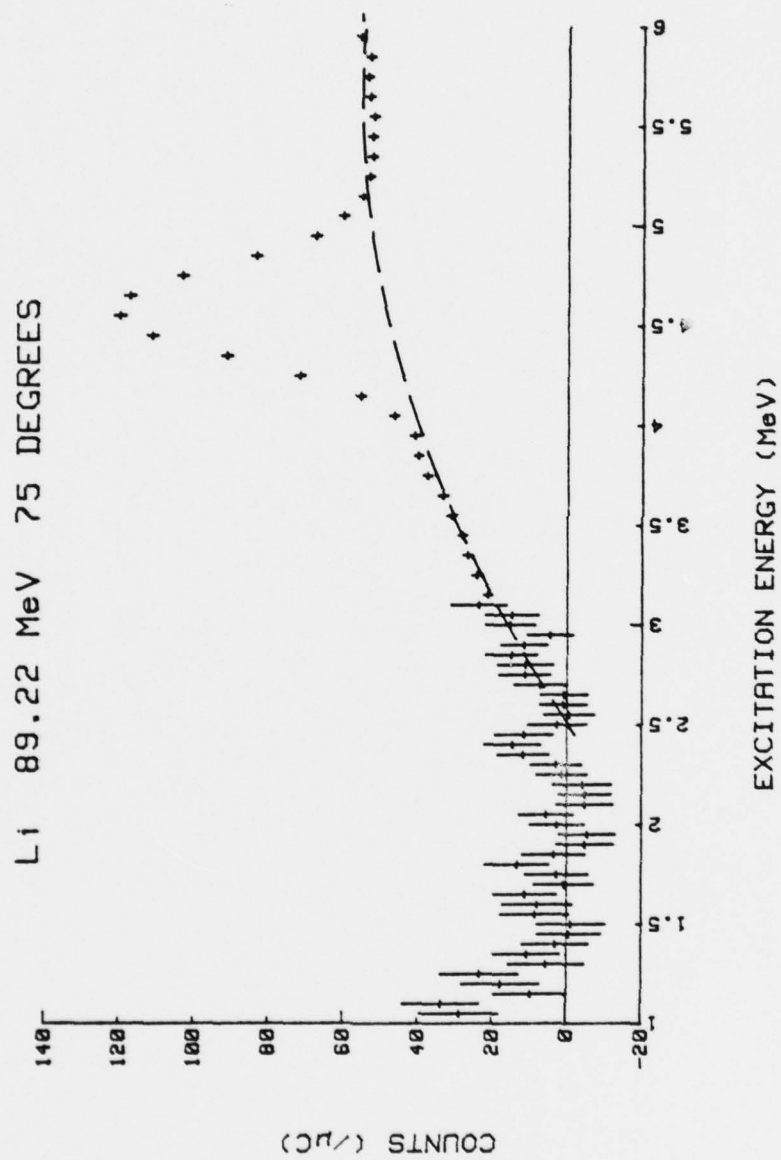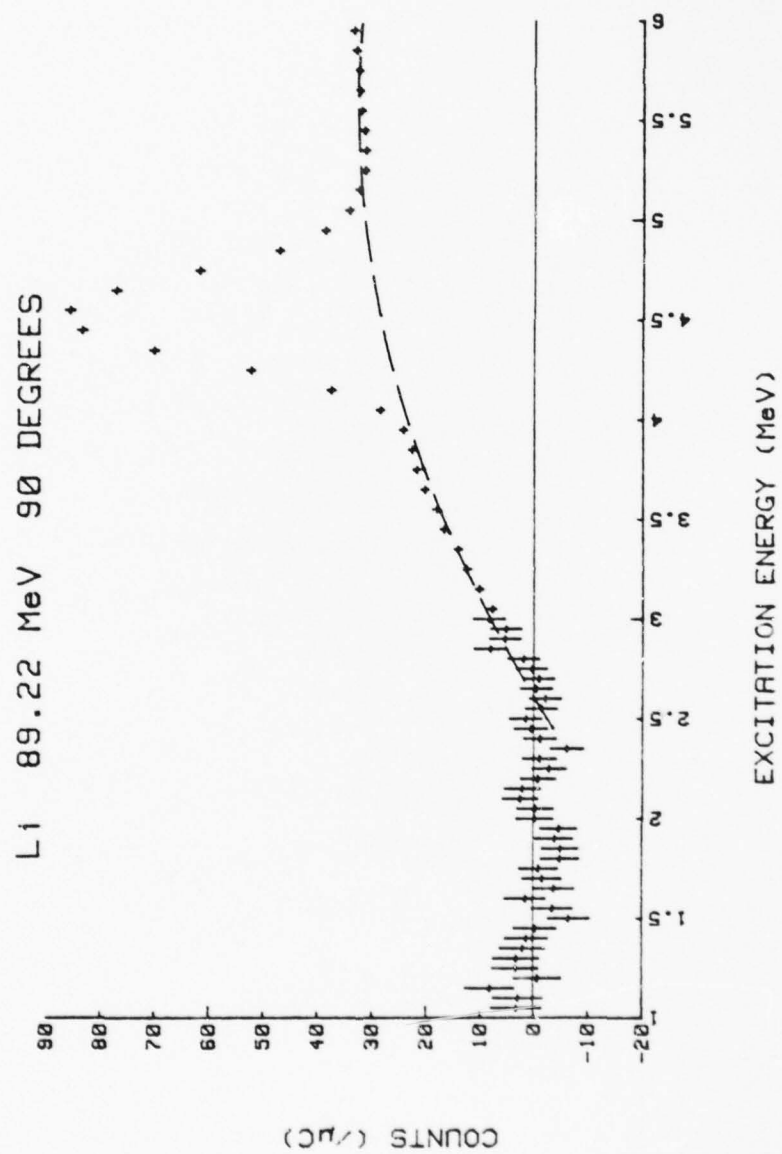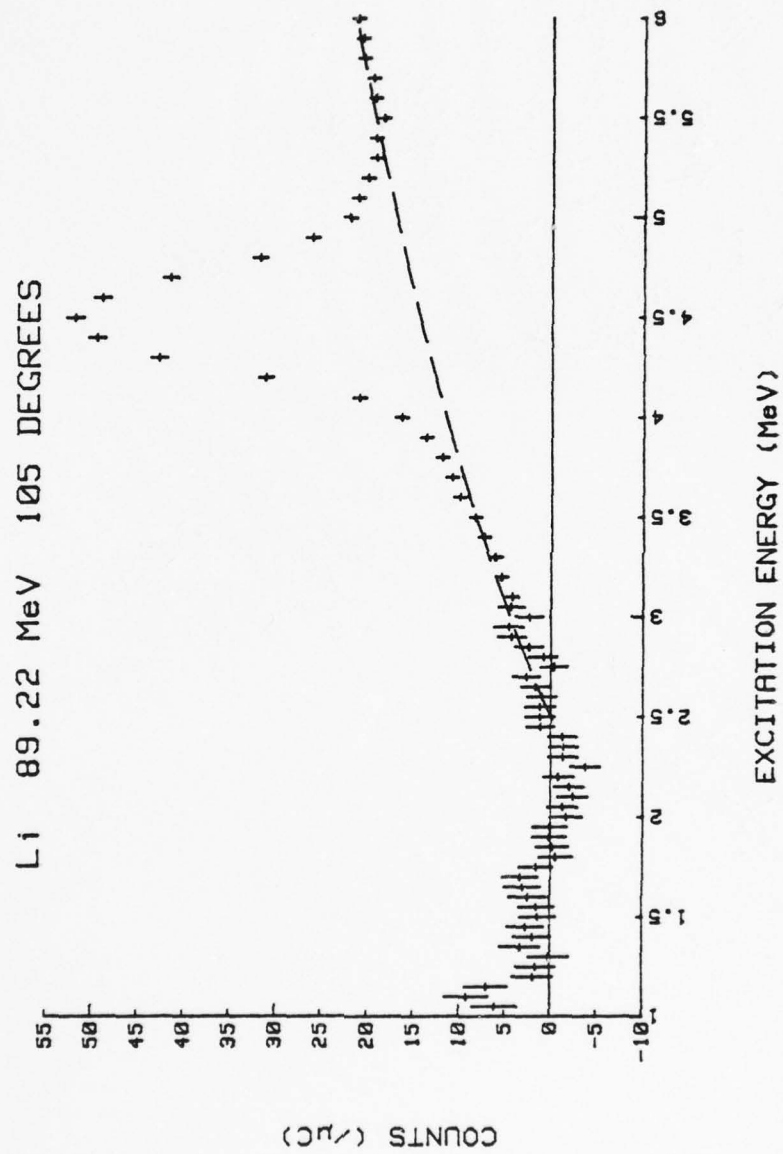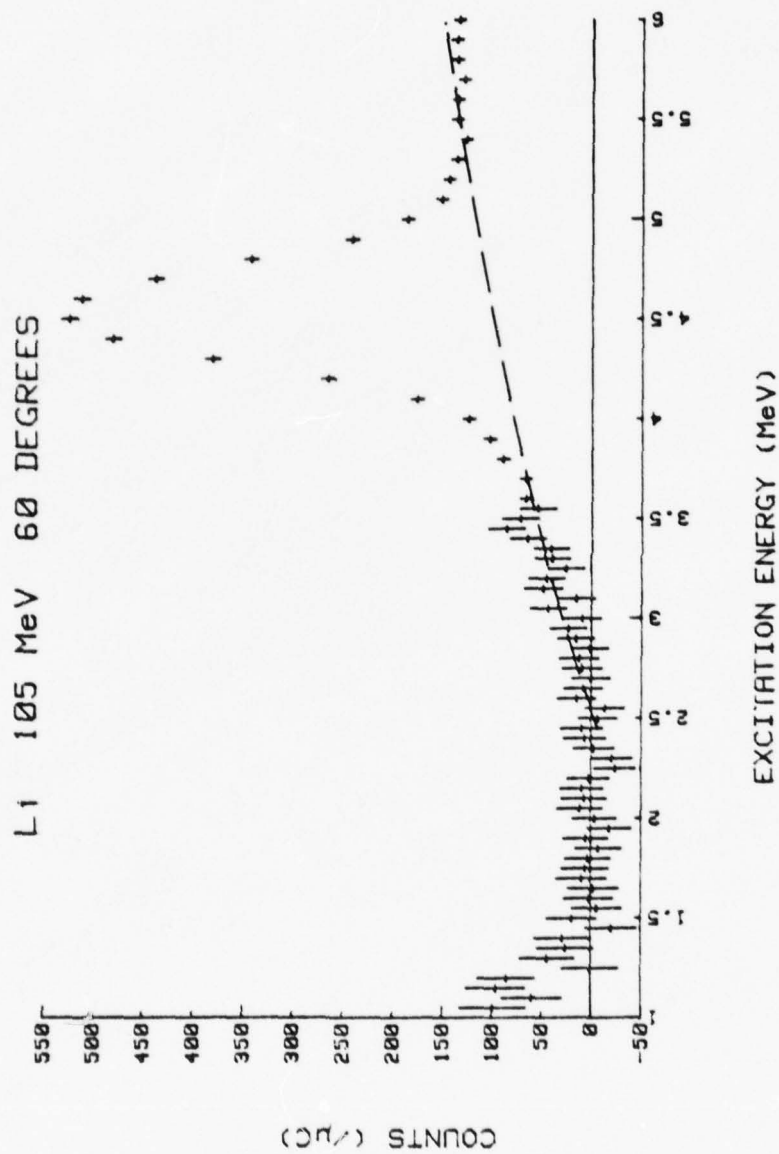
Li 89.22 MeV 75 DEGREES

COUNTS (/μC)

EXCITATION ENERGY (MeV)

Figure IV-10

38

Li 89.22 MeV 90 DEGREES

EXCITATION ENERGY (MeV)

COUNTS (/μC)

Figure IV-11

39

Li 89.22 MeV 105 DEGREES

COUNTS (/μC)

EXCITATION ENERGY (MeV)

Figure IV-12

40

Figure IV-13

41

Li 105 MeV 75 DEGREES

COUNTS (/µC)

EXCITATION ENERGY (MeV)

Figure IV-14

42

Figure IV-15

43

Figure IV-16

44

ELASTIC FORM FACTOR vs q²

+ 90 MeV DATA POINTS

* 105 MeV DATA POINTS

q²

F(q)

Figure IV-17

45

Figure IV-18

46

CONTINUUM FORM FACTORS vs q²

Figure IV-19

47
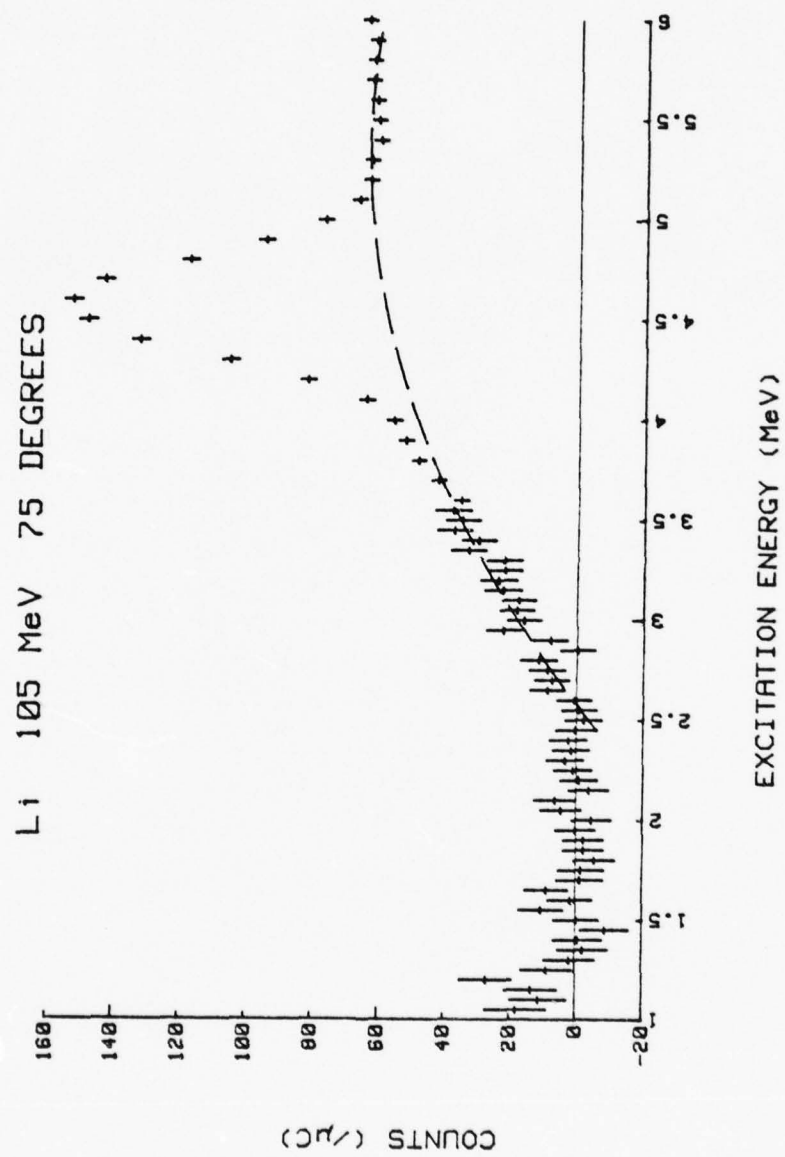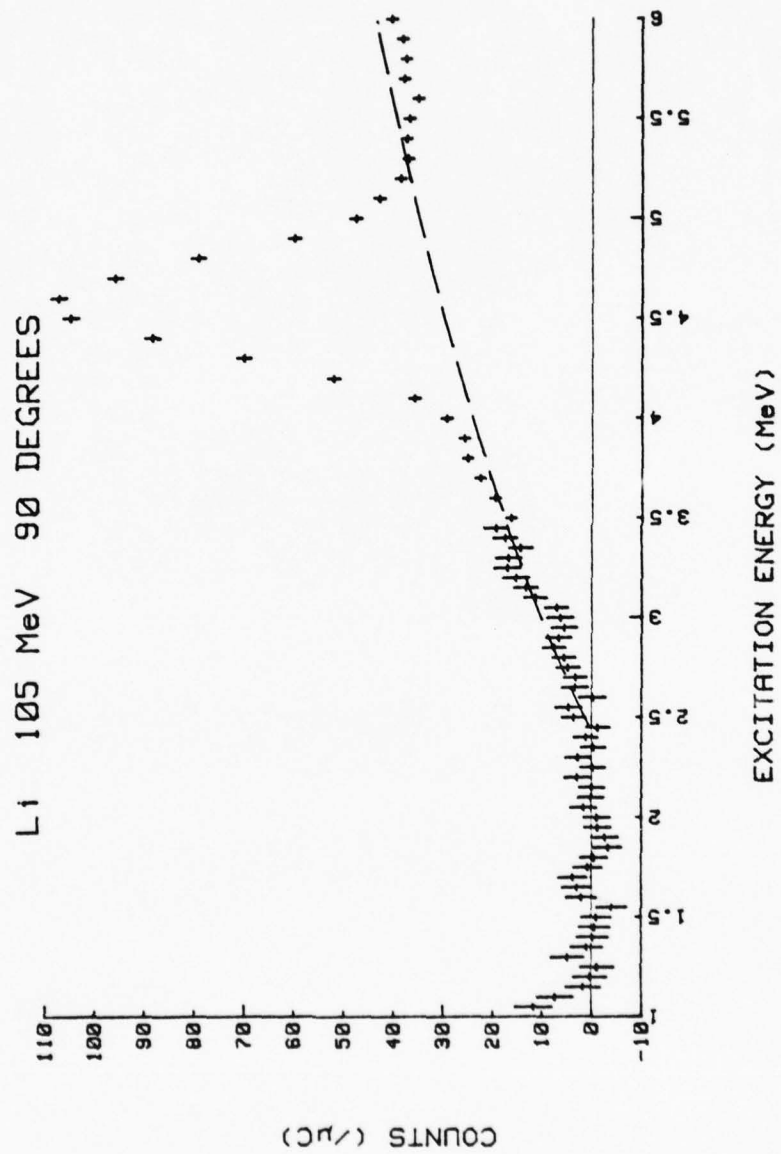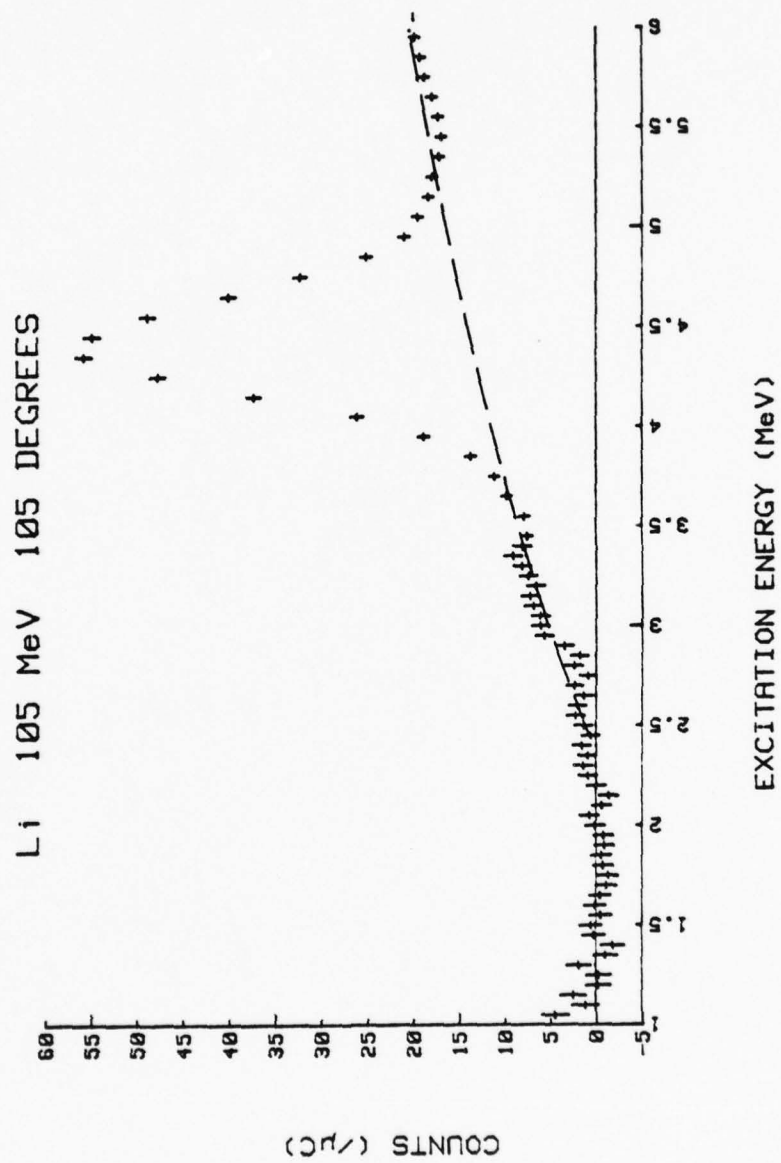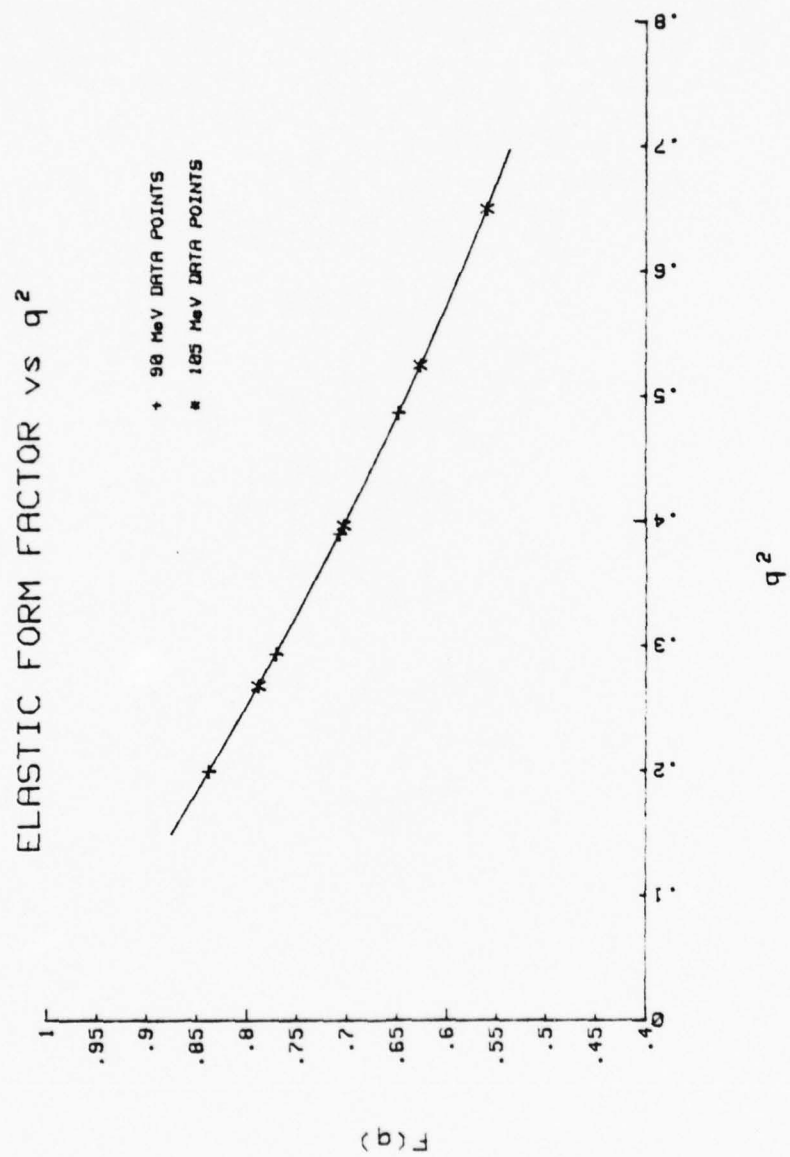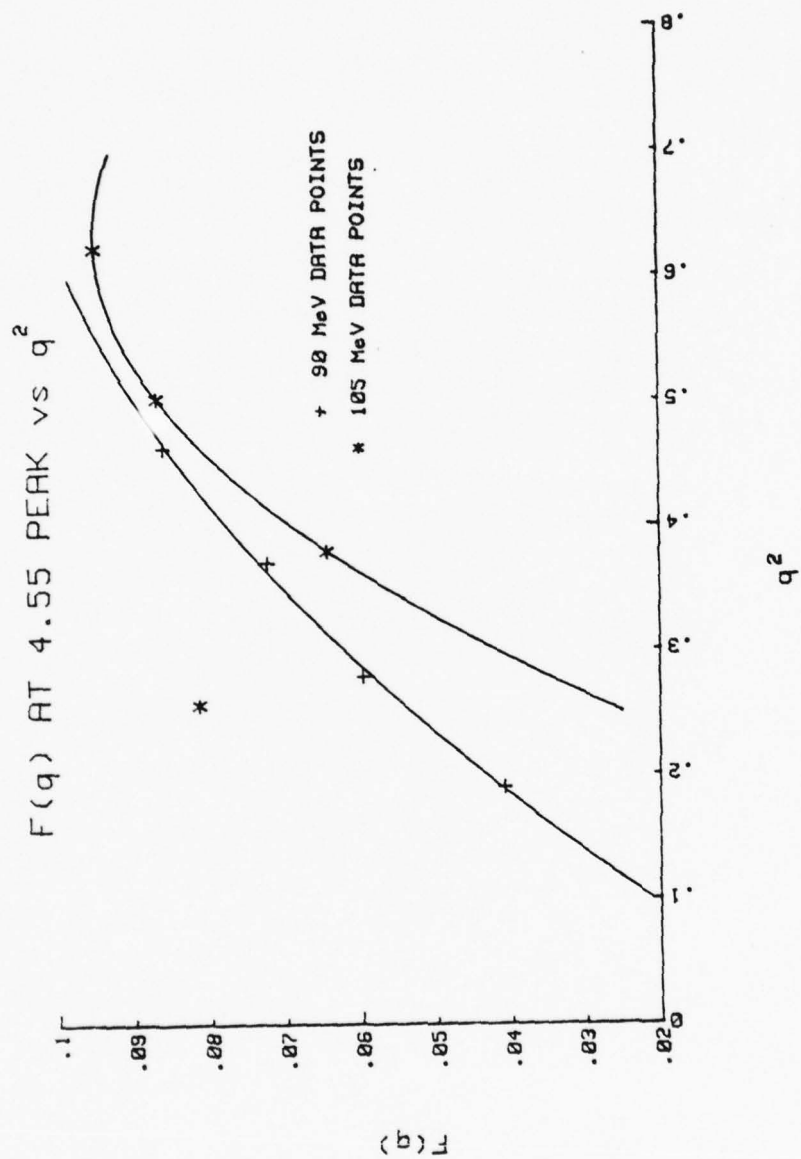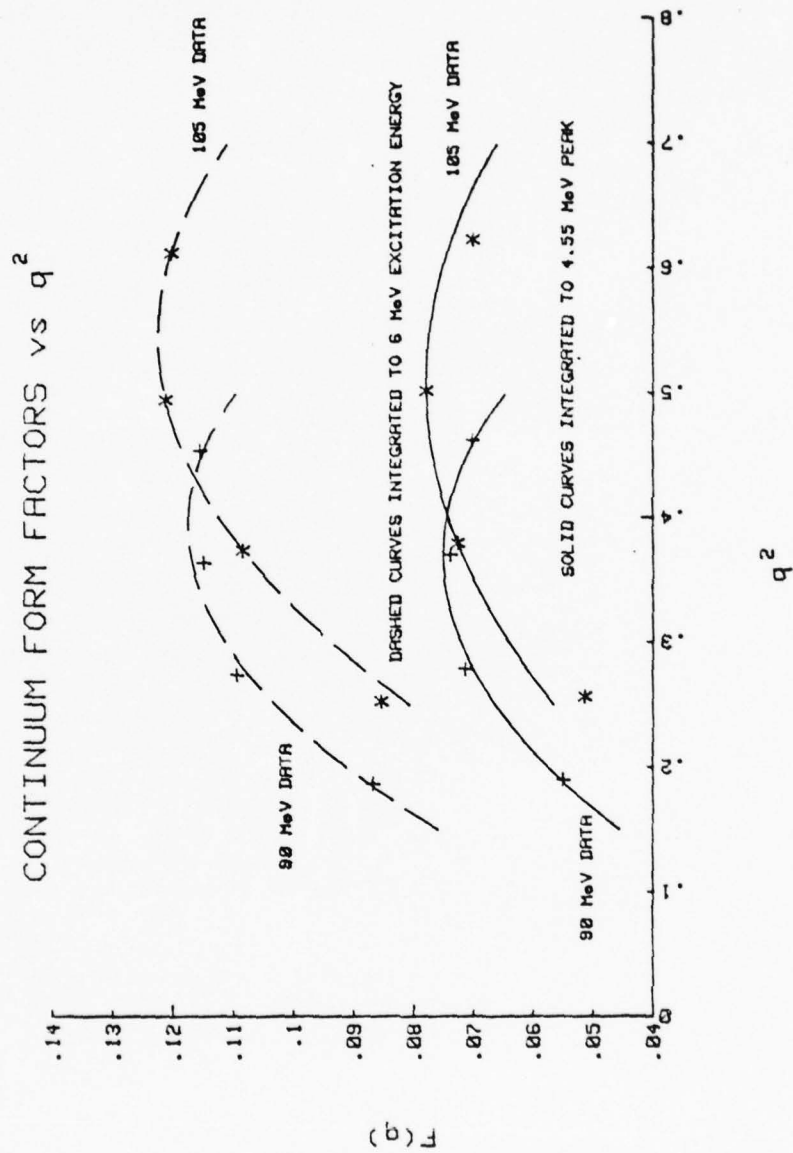
TABLE IV-1

ELASTIC SCATTERING PARAMETERS FOR ^{7}Li

(MeV)	θ	q^2 (F^{-2})	$F(q)$	$\left(\dfrac{d\sigma}{d\Omega}\right)_{Mott}$ (mb/sr)	$\left(\dfrac{d\sigma}{d\Omega}\right)$ (mb/sr)
89.47	60	.2000	.8378	3.871×10^{-1}	2.717×10^{-1}
105	60	.2682	.7885	2.881×10^{-1}	1.791×10^{-1}
89.22	75	.2935	.7709	1.484×10^{-1}	8.819×10^{-2}
89.22	90	.3902	.7072	6.527×10^{-2}	3.264×10^{-2}
105	75	.3969	.7030	1.094×10^{-1}	5.406×10^{-2}
89.22	105	.4868	.6486	3.060×10^{-2}	1.287×10^{-2}
105	90	.5251	.6267	4.830×10^{-2}	1.897×10^{-2}
105	105	.6501	.5600	2.280×10^{-2}	7.147×10^{-3}

TABLE IV-2

INELASTIC PEAK SCATTERING PARAMETERS FOR ^{7}Li

q^2 (F^{-2})	A_{in}/A_{el}	$\left(\dfrac{d\sigma}{d\Omega}\right)_{Mott}$ (mb/sr)	$F(q)$	$\left(\dfrac{d\sigma}{d\Omega}\right)$ (mb/sr)
.1898	2.374×10^{-3}	3.871×10^{-1}	4.082×10^{-2}	6.451×10^{-4}
.2565	1.065×10^{-2}	2.881×10^{-1}	8.133×10^{-2}	1.908×10^{-3}
.2785	5.986×10^{-3}	1.484×10^{-1}	5.965×10^{-2}	5.279×10^{-4}
.3703	1.104×10^{-2}	6.527×10^{-2}	7.224×10^{-2}	3.406×10^{-4}
.3793	8.377×10^{-3}	1.094×10^{-1}	6.434×10^{-2}	4.528×10^{-4}
.4622	1.757×10^{-2}	3.060×10^{-2}	8.598×10^{-2}	2.262×10^{-4}
.5018	1.918×10^{-2}	4.830×10^{-2}	8.679×10^{-2}	3.638×10^{-4}
.6227	2.871×10^{-2}	2.280×10^{-2}	9.487×10^{-2}	2.052×10^{-4}

TABLE IV-3

CONTINUUM PARAMETERS
(FROM THRESHOLD TO INELASTIC PEAK ENERGY)

q^2 (F^{-2})	A_{cont}/A_{el}	Integrated Cross Section (mb/sr)	$F(q)$
.1898	4.308×10^{-3}	1.171×10^{-3}	5.499×10^{-2}
.2565	4.239×10^{-3}	7.592×10^{-4}	5.134×10^{-2}
.2785	8.565×10^{-3}	7.553×10^{-4}	7.135×10^{-2}
.3703	1.091×10^{-2}	3.562×10^{-4}	7.388×10^{-2}
.3793	1.069×10^{-2}	5.778×10^{-4}	7.268×10^{-2}
.4622	1.171×10^{-2}	1.507×10^{-4}	7.013×10^{-2}
.5018	1.548×10^{-2}	2.936×10^{-4}	7.797×10^{-2}
.6227	1.571×10^{-2}	1.123×10^{-4}	7.017×10^{-2}

TABLE IV -4

CONTINUUM PARAMETERS
(FROM THRESHOLD TO 6 MeV EXCITATION ENERGY

$\dfrac{q^2}{(F^2)}$	A_{cont}/A_{el}	Integrated Cross Section (mb/sr)	$F(q)$
.1865	1.075×10^{-2}	2.922×10^{-3}	8.688×10^{-2}
.2526	1.175×10^{-2}	2.104×10^{-3}	8.545×10^{-2}
.2738	2.013×10^{-2}	1.775×10^{-3}	1.094×10^{-1}
.3638	2.644×10^{-2}	8.630×10^{-4}	1.150×10^{-1}
.3739	2.380×10^{-2}	1.287×10^{-3}	1.085×10^{-1}
.4539	3.175×10^{-2}	4.087×10^{-4}	1.156×10^{-1}
.4946	3.744×10^{-2}	7.102×10^{-4}	1.213×10^{-1}
.6122	4.619×10^{-2}	3.301×10^{-4}	1.203×10^{-1}

V.   RESULTS AND CONCLUSIONS

A.   COLLECTIVE RESULTS

Results of eight separate data runs (four at a primary electron energy of $\sim$ 90 MeV and four at a primary electron energy of 105 MeV and at scattering angles of 60, 75, 90 and 105 degrees) are depicted in Figures IV-1 through 19 and Tables IV-1 through 4. Due to an experimental energy resolution of 0.6%, the inelastic peak at 478 KeV could not be resolved. The figures show an inelastic continuum starting in the vicinity of the α -triton threshold (2.45 MeV excitation energy) and extending to higher excitation energies. An elastic peak which has previously been reported at 4.63 MeV [Ref. 2, 3, 4, 19] was found at 4.55 MeV excitation energy and its spectrum is superimposed on the inelastic continuum.

The curves for inelastic peaks and continuum cross sections are plotted separately for the different energies because form factors are not functions of q only if transverse multipoles are involved.

B.   4.55 MeV INELASTIC PEAK

As mentioned above, the 4.55 MeV inelastic peak (4.63 MeV) has been previously reported and analyzed on several occasions. Within the primary electron energy groups discussed above the ratio of the inelastic peak area to the elastic peak area and the inelastic form factors increase as q increases. The differential Mott and inelastic cross

52

section decrease as q increases. Experimental values are presented in Table IV-2 and plotted in Figure IV-18. The data run at 105 MeV with a scattering angle of 60° is an exception to these arguments and it will be discussed separately below.

C. INELASTIC CONTINUUM

As shown in Tables IV-3 and 4, the ratio of the continuum areas, integrated from threshold to 4.55 MeV excitation in the case of Table IV-3 and to 6 MeV excitation in the case of Table IV-4, to the elastic peak area increases as q increases in each primary electron energy group. The differential cross sections integrated over these limits decrease as q increases. As shown in Figure IV-19, the continuum form factors increase with q to a maximum and then decrease with increased q.

D. DISCREPANCY

As depicted in Table IV-2 and Figure IV-18, the ratio of the inelastic peak area to the elastic peak area for the 105 MeV, 60° run does not agree with values expected from an analysis of the other 105 MeV runs. In spite of this, the continuum cross section and form factors agree closely to those values predicted by extending the least squares line fit of the other 105 MeV runs down to the lower momentum transfer of this data run. The cause of this discrepancy has not been determined and should be investigated in the future. The parameters from this data point were not used in generating the line fits of Figures IV-18 and 19.

53

E. CONCLUSIONS

Results of these experiments are in general agreement
with results achieved by Bishop and Bernheim [Ref. 3] for a
different range of momentum transfer. The continuum observed
appears to be associated with the disintegration of ^{7}Li into
an alpha particle and a triton. Data presented herein should
be further analyzed in an effort to draw conclusions in terms
of various nuclear models and multipole transitions.

APPENDIX A

COMPUTER PROGRAMS

A.   ASC

Code ASC is a revision of the Code KIK described in detail by Warshawsky and Webber [Ref. 20]. This revision allows up to 599 data sets to be processed. The input parameters of each data set are discussed below. ASC compiles the separate spectra of the ten counting channels into one combined spectrum showing energy (MeV), count rate (counts/microcoulomb) and error (counts/microcoulomb).

The set up of a FORTRAN card deck to use Code ASC consists of the appropriate control cards, four parameter cards, the data deck and two trail cards. When using the Control Program/Cambridge Monitor System (CP/CMS) at the NPS Computer Facility, two files are required. A FT04F001 file serves as the data set file and a FT05F001 file serves as the parameter file. In the description which follows the numbered headings refer to separate parameter cards in the FORTRAN deck or separate lines in FT05F001 as appropriate. FORTRAN formats appear in parentheses. Parameters marked by an asterisk are optional and may be left blank.

    1.   TEXT   Identifying alphanumeric remarks   (20A4)

    2.   ENGUP, ENGLOW, DENG, TAU, SUMCHK   (5F10.5)

        ENGUP   Upper spectrometer energy limit for the spectrum in MeV.

        ENGLOW   Lower spectrometer energy limit for the spectrum in MeV.

55

DENG   Spectrometer energy step width in MeV.
ASC interpolates to generate missing
data sets.

TAU*   Counting system dead time/pulse length.

SUMCHK* = 0. ASC will then inform user when the
total counter sum is incorrect in the
particular data set.

3. N(1)...N(10)   (10I4)
Spectrometer counting system normalization
factors relative to counter number 6. The
N(i)'s are defined as

$$N(i) = \left[\frac{Energy(6)}{Energy(i)} - 1 \right] \times 10^4$$

4. LU, LO, INV, FKXAD, FKEN   (3I10,2F10.5)

LU*, LO* The spectrum of counter J, LU J LO will
be punched out onto cards.

INV   If INV 0, then the order of the input data
sets is reversed; i.e. from lower to higher
energies.

FKXAD   When 0 the input capacitor voltage (at
full scale) will be scaled to units of 10^{-3}
volts with multiplication by this factor.
For the NPS LINAC, FKXAD = 0 defaults and
the voltage is recorded in millivolts.

FKEN   The input energy will be scaled to units
of KeV when multiplied by this factor. For
the NPS LINAC, FKEN = 1.014.

Data cards now follow with two cards comprising a data set.

Input parameters are in the order recorded on the magnetic

tape as described in Section II-D and are as follows:

Card 1: XHZ,MIVOLT,EO,MUEF,XIP,XAD,DUM1,ZESS(1)...
ZESS(3)   (10F7.0)

Card 2: ZESS(4)...ZESS(10),UNTZ,DUM2,SUM10(10F7.0)

XHZ   Spectrometer energy setting (MeV)

MIVOLT Full scale voltage setting of
capacitor (mv)

56

EO	Incident accelerator energy (MeV),
MUEF	Capacitance of collecting capacitor (MF).
XIP	Elapsed time (sec),
XAD	Final voltage on the cpacitor (mv),
DUM1	Spectrometer "accidentals" counter,
ZESS(I)	Counts registered in "ith" counter,
UNTZ	Spectrometer backing counter number 11 reading,
DUM2	Spectrometer backing counter number 12 reading.
SUM10	Total counts registered in counters 1 through 10.

5. Trail cards   (10F7.0)

(Same format and parameters as data cards in 4 above).
When a card is encountered with columns 1-7 blank, it and the
next card are considered trail cards and parameter values for
ZESS(I) are given the following meaning:

ZESS(I)   If $\neq$ 0, then counter number will not be considered when compiling the total spectrum.
The value of N(I) on parameter card 3 above must also = 0.

When using CP/CMS a FT04F001 file is used as a data file
and the trail cards are entered as two additional lines at
the end of this file. All formats are the same.

A sample of the parameter cards and data deck for a hypothetical run at 90 MeV machine energy with a scattering
angle of 75 degrees follows. The dashed line separates the
parameter cards (FT05F001 file) from the data deck (FT04F001
file) for purposes of clarification only. The two blank

57

trail cards at the end of the data deck indicate that all
counters were used.

SAMPLE

LI 90 EL(90 MEV, 100 SLITS, 75 DEG., 144.0MG/CM**2) 6 JAN 79
 90.0   81.5   .05
 2050 1600 1130   730   350   0 -330 -730-1020-1390

                                          1.014

090.00 001000 090.00 0054.3 030122 000000 000007 000004 000004

000003 000004 000002 000001 000000 000000 000782 000542 000025

... (Rest of data deck follows) ...

(Blank trail card)

(Blank trail card)

B. HP 9845A PROGRAMS

Simple computer programs were written for use on a
Hewlett-Packard Model 9845A Computer. These programs stored
the spectrum output from Code ASC onto cassette tape data
files with separate data files for the spectrum data and upper
and lower error bounds for each of the runs. One program
using the equations presented in Section IV-A and B computed
the elastic peak radiation tail for each run and stored this
on cassette data files. Another program subtracted the radi-
ation tail from the spectrum data and error bound files for
each run and created additional files to store this data.
Appropriate data files were accessed by a plotting routine
and graphs were drawn using a Hewlett-Packard Model 9872A
Plotter.

The Hewlett-Packard program "REGS" [Ref. 21] was used as a fitting routine to determine the equations for the line fit to the inelastic continuum. This program provides the option of specifying a linear, logarithmic, expotential or polynomial of desired degree.

BIBLIOGRAPHY

1. Berhnheim, M. and Bishop, G. R., Le Journal De Physique
    24, 970 (1963).

2. Berhnheim, M. and Bishop, G. R., Phys. Lett. 5, 294
    (1963).

3. Bishop, G. R. and Bernheim, M., Phys. Lett. 5, 48 (1963).

4. Hutcheon, R. M. and Caplan, H. S., Nuc. Phys. A127,
    417 (1969).

5. Bergstrom, J. C. and Tomusiak, E. I., Nuc. Phys. A262,
    196 (1976).

6. Monson, W. A., NPS Thesis, June 1969.

7. Mott, N. F., Proc. Roy. Soc. (London) A124, 425 (1929).

8. Hofstadter, R., Electron Scattering and Nuclear and
    Nucleon Structure, Benjamin, New York (1963).

9. Barber, W. C., Ann. Rev. of Nuc. Sci. 12, 1 (1962).

10. Theissen, H., Spectroscopy of Light Nuclei by Low Energy
    (70 MeV) Inelastic Electron Scattering, Institut fur
    Technishe Kernphysik der Technischen Holschule, Darmstadt
    (1972).

11. Isabelle, D. B. and Bishop, G. R., Nuc. Phys. 45, 209
    (1963).

12. Barber, W. C., Berthold, F., Fricke, G., and Gudden,
    F. E., Phys. Rev. 120, 2081 (1960).

13. Chodorow, M., et al., Rev. of Sci. Inst. 26, 134 (1955).

14. Schwinger, J., Phys. Rev. 75, 898 (1949).

15. Tsai, Y. S., Phys. Rev. 122, 1898 (1961).

16. Bethe, H. A. and Ashkin, J., Experimental Nuclear
    Physics, John Wiley and Sons, Inc., New York (1953).

17. Bumiller, F. A., Buskirk, F. R. and Dyer, J. N., Phys.
    Rev. 5, 391 (1972).

18. Schiff, L. I., Phys. Rev. 87, 750 (1952).

19. Suelze, L. R., Yearian, M. R. and Crannell, H., Phys. Rev. <u>162</u>, 992 (1967).

20. Warshawsky, A. S. and Webber, A. M., NPS Thesis, *December* 1973.

21. Hewlett-Packard Calculator Products Division, <u>Hewlett-Packard System 45 Software, General Utility Routines</u>, Rev B., 1977.

INITIAL DISTRIBUTION LIST

                                                    No. Copies

1. Defense Documentation Center   2
    Cameron Station
    Alexandria, Virginia 22314

2. Library, Code 0142   2
    Naval Postgraduate School
    Monterey, California 93940

3. Physics Library, Code 61   2
    Department of Physics and Chemistry
    Naval Postgraduate School
    Monterey, California 93940

4. Professor F. R. Buskirk, Code 61Bs   5
    Department of Physics and Chemistry
    Naval Postgraduate School
    Monterey, California 93940

5. Professor J. N. Dyer, Code 61Dy   2
    Department of Physics and Chemistry
    Naval Postgraduate School
    Monterey, California 93940

6. Professo W. R. Pitthan, Code 61Pt   2
    Department of Physics and Chemistry
    Naval Postgraduate School
    Monterey, California 93940

7. Cpt. Robert F. Ryan, U.S.A.   1
    FAOAC 4-79
    Officer Student Battalion
    Fort Sill, Oklahoma 73503